

Wavelet Policy: Imitation Policy Learning in the Scale Domain with Wavelet Transforms

Changchuan Yang¹, Yuhang Dong¹, Guanzhong Tian^{1,3}, Haizhou Ge², and Hongrui Zhu¹

Abstract—Recent imitation learning policies, often framed as time series prediction tasks, directly map robotic observations into the action space, such as high-dimensional visual data and proprioception. When deploying at the edge, we found the underutilization of frequency domain analysis in robotic manipulation trajectory prediction leads to neglecting the inherent rhythm information embedded within action sequences, resulting in errors at critical moments. To address this, we reframe imitation learning policies through the lens of time-scale domain and introduce the Wavelet Policy. This novel approach employs wavelet transforms (WT) and new Features Extractor (FE) for feature preprocessing and extracts multi-scale features using the Single Encoder to Multiple Decoder (SE2MD) architecture. Furthermore, to enhance feature mapping in the scale domain and appropriately increase model capacity, we introduce a Learnable Scale Domain Filter (LSDF) after each decoder, improving adaptability under different visual conditions. Our results show that the Wavelet Policy maintaining a comparable parameter count outperforms SOTA end-to-end methods on four challenging simulation robotic arm tasks and real tasks, especially at critical moments and remote settings simultaneously. We release the source code and model checkpoint of simulation task at Wavelet.Policy.

I. INTRODUCTION

Imitation learning has emerged as a leading approach for training robots in manipulation tasks [1]. Typically framed as time-series prediction problems, policies aim to map raw observations to actions [2]. This process often depends on 2D or 3D spatial-domain modeling to capture relationships in the data. We find that traditional 3D point-cloud and 2D image mappings suffer from an inherent information bottleneck, making it difficult to directly optimize these representations for better performance. As illustrated in Fig. 1, we assessed ACT [3] on four datasets with two metrics: joint-angle error and the level-1 term of a wavelet-transform multi-scale error. Comparable behavior emerged at the remaining scales and likewise for other sequence-modeling architectures. Under otherwise identical settings, once the model began to overfit, its overall success rate declining by about 10% from its optimum. The joint-level error dropped markedly, whereas the multi-scale error showed only marginal improvement. Besides, as shown in Fig. 4, our frequency-domain analysis re-

TABLE I: The SE2MD structure significantly reduces model complexity, requiring about one-third of the parameters of comparable methods.

Model	Visual Backbone: ResNet-18		
	Params	Encoder Layers	Decoder Layers
DP (DDPM, CNN) [1]	308.29M	-	-
DP (DDIM) [6]	77.55M	-	-
ACT	83.92M	4	6
NL-ACT [2]	84.32M	4	7
InterACT [7]	67.70M	3	4
HACT-VQ [8]	125.49M	-	-
Ours (one cam)	17.22M	2	2
Ours (two cams)	24.41M	4	8

veals that the ACT model as well as other sequence-modeling architectures exhibits significantly larger multi-scale errors at key instants compared to its performance during steady-state operation. This pattern indicates that the network allocates disproportionate attention to temporal cues and lacks sufficient sensitivity to errors across different spatial scales, which are crucial for accurate trajectory prediction in robotic manipulation. While traditional time-series prediction [4], [5] has largely focused on spatial relationships, the frequency domain remains an underutilized resource in this context. The lack of frequency domain analysis may hinder the ability of model to capture the rich rhythm information embedded within sequential actions, potentially limiting performance and efficiency, particularly in more complex and long-range tasks.

In this work, we propose Wavelet Policy, a novel method that utilizes WT [9] for multi-scale frequency-domain processing and efficient end-to-end trajectory prediction. At the heart of our approach is the FE and SE2MD architecture, which is tailored for multi-scale feature processing and can efficiently transform global features from images into specific visual features of target action sequences across various scale domain. We leverage a discrete WT to decompose visual features into different frequency bands, then use a transformer-based SE2MD architecture to encode shared representations and decode motions at multiple scales. Additionally, we design LSDF modules after each decoder to adaptively refine the scale-specific features and improve robustness under varying visual conditions. Notably, as shown in Table I, our architecture requires only about one-third the parameters of comparable models, making it well-suited for lightweight, edge deployment. This reduction in model size is achieved without sacrificing performance.

*This work is supported in part by the National Natural Science Foundation of China under Grant 62303405, in part by the Ningbo Natural Science Foundation Project under Grant 2023J400, and in part by the Ningbo Key Research and Development Plan under Grant 2023Z116. This work is also supported by Hangzhou TaiWeave Robotics Co., Ltd., through experimental assistance with the industrial sewing setup and xArm6 industrial manipulator from UFactory.

¹Zhejiang University

²Tsinghua University, DISCOVER Robotics

³Corresponding author: gztian@zju.edu.cn

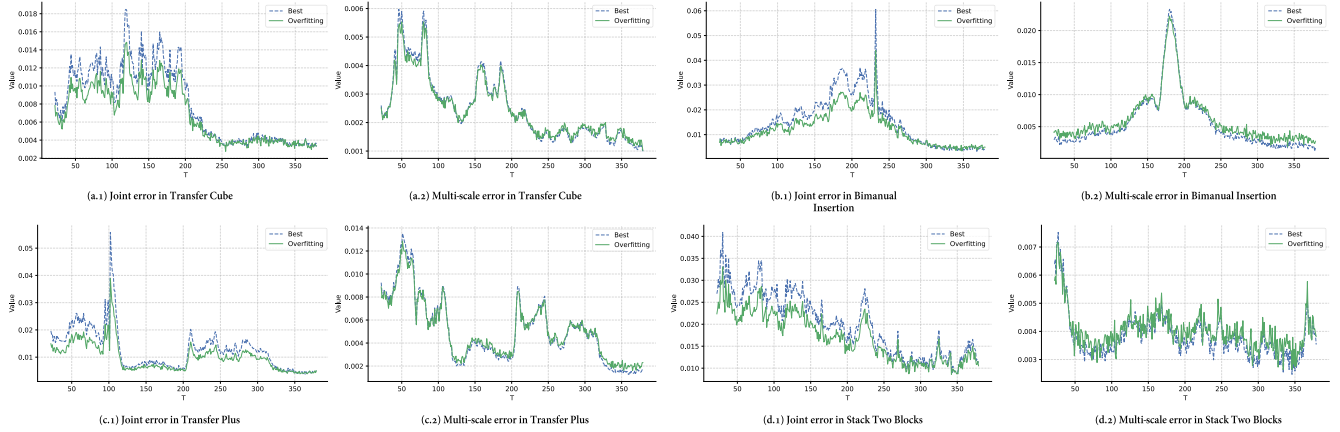


Fig. 1: We evaluated the ACT model, and observed a similar tendency in other sequence-based architectures.

Our main contributions are summarized as follows:

- **Efficient Feature Extraction.** We devise a lightweight ResNet-based front-end that rapidly compresses raw visual features into a compact token sequence.
- **Multi-Scale Domain Analysis and SE2MD Architecture** After a WT-based scale domain analysis pipeline, we propose a model architecture with multiple decoders and a single encoder.
- **Learnable Scale Domain Filter:** We design a trainable filter to dynamically adjust feature representations across varying visual conditions, enhancing feature mapping in the scale domain and increasing model capacity controllably.
- **Edge device deployment experiment:** We deployed our model on robotic arm, and the task completion rate was significantly improved compared to the ACT model.

II. RELATED WORKS

A. Imitation Learning

Imitation learning has become a cornerstone of robotics [10], [11], [12], enabling agents to mimic expert demonstrations for complex tasks such as robotic arm manipulation. Techniques like Behavioral Cloning [13], [14], [15] and Inverse Reinforcement Learning [16], [17] are commonly used to learn policies directly from demonstrations. Recent advancements have integrated imitation learning with deep learning frameworks [18], [19], employing architectures such as transformers [20], [21] and recurrent networks [22] to handle sequential decision-making. Robotic arm manipulation, including tasks such as object grasping [23], pick-and-place [24], and trajectory tracking [25], remains a central challenge in embodied intelligence. However, these conventional methods typically operate purely in the time domain and thus ignore the intrinsic rhythm of manipulation motions, which is the frequency content.

B. Feature Processing in Robotics

Feature processing plays a pivotal role in robotics, bridging raw sensory inputs and actionable representations. While modern deep learning techniques, such as convolutional networks [26], [27] and attention mechanisms [28], [29], improve performance, they often have limited ability to improve model efficiency by capturing multi-scale dependencies, and essentially they are a link in the decreasing information entropy of the model. The traditional 3D point clouds and 2D image direct map [30] suffer from inherent information entropy loss, making it more difficult to directly optimize these processes to improve model performance.

C. WT: Wavelet Transform

WT are powerful tools in signal processing because they decompose data into frequency components that are simultaneously localized in time and space, enabling true multi-resolution analysis [31]. Unlike global Fourier transforms which lack temporal localization and can suffer from aliasing or gradient leakage, wavelets offer local time–frequency representations that enable perfect signal reconstruction without information loss. Due to their ability to capture both fine-grained details [32] and broader contextual structures [33], WT are particularly well suited to analyzing complex signals [34]. In computer vision, they have achieved notable success in texture analysis [35], [36], image compression [37], [38], and feature extraction [39], [40]. The orthogonality of wavelet basis guarantees perfect signal reconstruction without loss of information entropy or notable computational overhead, while also providing rich multi-scale features for downstream models.

III. METHODS

A. Overview

Given RGB images as multi-view visual observations at the current time step, our goal is to predict a 40-step sequence of future joint angles for a robotic manipulator. To achieve this, Wavelet Policy is designed with three key

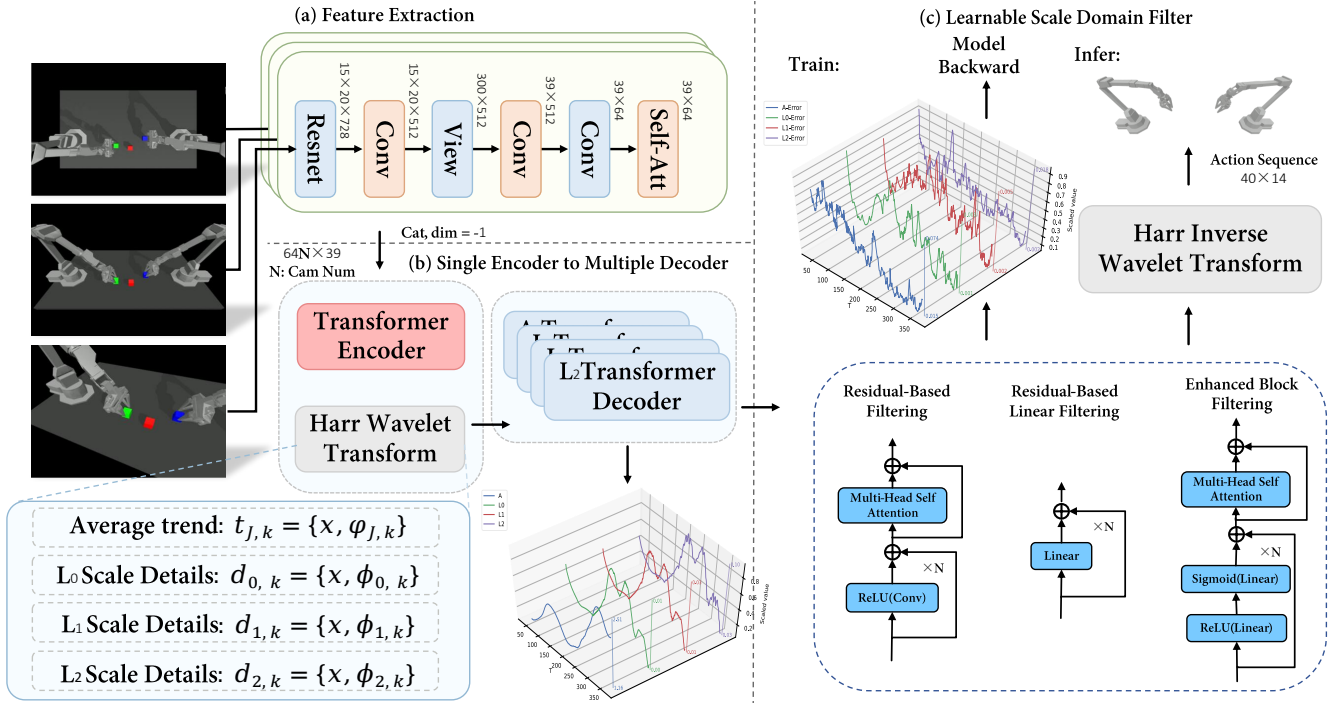


Fig. 2: Wavelet Policy employs a modular design with three key components: a FE module for initial visual processing, the SE2MD structure for multi-scale representation via a wavelet-based encoder–decoder framework, and the LSDF modules for task-specific feature refinement.

components as shown in Fig. 2: (a) a **Feature Extraction (FE)** module that processes raw images into a compact token representation, (b) a **Single Encoder to Multiple Decoders (SE2MD)** transformer network that operates in the scale domain to generate multi-scale trajectory predictions, and (c) a **Learnable Scale-Domain Filter (LSDF)** applied to each decoder’s output for task-specific feature refinement. We describe each component below.

B. FE: Feature Extraction

The purpose of Feature Extraction is to quickly and efficiently compress feature information from Resnet to adapt to downstream feature processing. The visual front-end converts each RGB frame into a compact sequence of tokens suitable for SE2MD processing.

Given an input image, a truncated ResNet-18 yields a spatial feature map of size $15 \times 20 \times 728$. Batch-normalisation layers are frozen to stabilise training. We then apply a 1×1 channel-squeeze that reduces the width from 728 to 512, preserving spatial fidelity yet trimming FLOPs. The 15×20 grid is flattened into $L = 300$ patch tokens and processed by two lightweight 1-D convolutions:

Here we utilize token condensation and function projection to further compress features efficiently. A single 1-D convolution with $\text{kernel_size} = 3$ maps the patch dimension $\mathbb{R}^{B \times 300 \times 512} \rightarrow \mathbb{R}^{B \times 39 \times 512}$, acting as a learnable substitute for hand-crafted subsampling. A second 1-D convolution, also with $\text{kernel_size} = 3$, projects the channel width from 512 to 64, producing $\mathbb{R}^{B \times 39 \times 64}$. A single multi-head self-attention layer then carries out early cross-token mixing,

fusing local cues and global context at negligible cost. For multi-view setups the entire pipeline runs in parallel and the resulting sequences are concatenated along the last token axis, yielding a tensor of shape $64N \times 39$.

Overall, the SOTA of the experimental results indicates that the pipeline removed approximately 93% of the redundant features from the original ResNet that is not required in robotic arm operations.

C. SE2MD: Single Encoder to Multiple Decoders

In order to fully utilize the multi-scale domain information, the Discrete WT is implemented in our framework to decompose the input tensor from FE. At each decomposition level, the WT produces low-pass and high-pass components. This operation is recursively applied for J levels. In our proposed framework, HWT is used to analyze and encode multi-scale features for robotic motion prediction. HWT decomposes the input signal x into one low-frequency *average trend* $t_{J,k} = \{x, \varphi_{J,k}\}$ and a set of multi-scale *detail components* $d_{0,k} = \{x, \phi_{0,k}\}$, $d_{1,k} = \{x, \phi_{1,k}\}$, and $d_{2,k} = \{x, \phi_{2,k}\}$.

The encoder in the SE2MD framework is built upon transformer encoder layers, which process a sequence of features derived from FE. The encoder outputs a shared latent representation $H \in \mathbb{R}^{T \times D}$, which is subsequently used by multiple decoders for downstream processing. Specifically, for each scale $j \in \{1, 2, 3\}$, a dedicated transformer decoder



Fig. 3: Left: The MuJuCo tasks *Transfer Cube*, *Bimanual Insertion*, *Transfer Plus*, and *Stack Two Blocks*. Right: The real-world tasks *Stack Block*, *Store Strawberry*, *Store Lemon*, *Store Items*, *Assist Sewing*, and *Stack Blocks*.

takes the pair $(t_{J,k}, H)$ and $(d_{j,k}, H)$ as input:

$$y_t^{(j)} = \begin{cases} \text{Decoder}_0(t_{J,k}, H), & j = 0, \\ \text{Decoder}_j(d_{j-1,k}, H), & j = 1, 2, \dots, J. \end{cases} \quad (1)$$

In our framework, the outputs of the decoders are passed through the fully connected layers built by linear layers. Then, Let $\tilde{t}_{J,k} = y_t^{(0)}$ denote the low-frequency prediction produced by the trend decoder, and let $\tilde{d}_{j,k} = y_t^{(j)}$ ($j = 1, \dots, J$) be the scale-specific detail predictions. Starting from the coarsest level J , we recursively apply a one-dimensional synthesis filter bank $\text{SFB1D}(\cdot, \cdot; g_0, g_1)$ —i.e. the inverse Haar transform—to merge each pair of coefficients:

$$\tilde{t}_{j,k} = \text{SFB1D}(\tilde{t}_{j+1,k}, \tilde{d}_{j+1,k}; g_0, g_1), \quad (2)$$

where g_0 and g_1 are the Haar synthesis filters. Then, we obtain $\hat{x}_k = \tilde{t}_{0,k}$, a unified trajectory that combines all multi-scale components for downstream control.

D. LSDF: Learnable Scale-Domain Filter

In our framework, to enhance feature mapping in the scale domain and controllably increase model capacity, we introduce LSDF including Residual-Based Filtering (RBF), Residual-Based Linear Filtering (RBLF) and Enhanced Block Filtering (EBF). They dynamically refine the wavelet-transformed features for each scale band. This design addresses the challenges posed by diverse and dynamic visual conditions, enabling the model to adaptively adjust feature representations across different scale domains. The learnable filter is integrated into each decoder of the SE2MD architecture, improving the frequency-specific processing capabilities of framework. Each decoder in the SE2MD architecture incorporates a learnable filter tailored to its assigned frequency band. The filter dynamically adjusts the wavelet coefficients before further processing, enhancing the adaptability of the framework. Specifically, the wavelet coefficients $y_t^{(j)}$ for the j -th scale band are processed by the selected learnable filter to produce a refined representation. The filtered coefficients are then passed to the corresponding fully connected layer for downstream motion prediction. Moreover, LSDF is constructed using residual structures, and the controllable increase in model capacity can be achieved by specifying the value of N .

IV. EVALUATION

A. Experimental Setup

We evaluated Wavelet Policy on four simulated robotic arm tasks and six real-world tasks, as illustrated in Fig. 3.

In the simulation benchmarks, Transfer Cube and Bimanual Insertion are taken from [3], while Transfer Plus and Stack Two Blocks are new, more challenging tasks we designed. Transfer Plus extends the cube transfer task by requiring the robot to stack the transferred cube onto another block, and Stack Two Blocks requires two arms to sequentially stack two blocks together. The left side of Fig. 3 shows these simulation scenarios. For real-world evaluation, we deploy our policy on two platforms. The Airbot Play is used for block stacking and item storage tasks, while the UFactory xArm6 is used for an assisted fabric feeding task and a multi-step block stacking task.

All simulated experimental results, including ablation studies and experiment on IV-B, IV-C and IV-D, are obtained by averaging over 10 random seeds. For each seed, training is performed for 100k iterations on 100 training episodes per task. The checkpoint achieving the best validation performance is then evaluated on 100 test episodes, and the final reported result is the average across the 10 such evaluations. Unless stated otherwise, Wavelet Policy uses a single camera view and no LSDF filters (i.e., the base model). Training was performed on an NVIDIA RTX 3090, and inference timing was measured on an NVIDIA GTX 1650.

B. Simulation Results

We compare Wavelet Policy to five baseline approaches: Diffusion Policy (DDPM, CNN) [1], ACT [3], NL-ACT [2], InterACT [7], and HACT-VQ [8]. We first conducted comparative experiments on models without Learnable Filters. As shown in Fig. 4, we tested the 1st scale domain error values (with similar errors in other scale domains) of the model on a expert-demonstration dataset. Wavelet Policy has improved in terms of error compared to the ACT model. The Figure indicates that scale domain information represents important control rhythm information for the robotic arm, which directly affects the success or failure of the task.

Our findings in TABLE II show that our model outperforms SOTA models by approximately 2% on challenging tasks such as Bimanual Insertion and Stack Two Blocks. In long-horizon tasks, such as Transfer Plus, which extends the Transfer Cube task by adding a stacking operation, ACT exhibits a 28% drop in success rate when compressing task execution time, with an additional 9% decrease when incorporating the stacking block task. In contrast, our model experiences only a 19% and 8% drop, respectively, demonstrating a slower decline in performance as task complexity increases. These results suggest that our model excels in long-horizon tasks. We attribute superior performance of our policy to the role of WT in extracting global features that are more interpretable for transformers. Additionally,

TABLE II: Comparison of Wavelet Policy with five baseline models. Success rate (%) \uparrow .

	Transfer Cube (Sim)			Bimanual Insertion (Sim)			Transfer Plus (Sim)			Stack Two Blocks (Sim)		
	Touch	Lift	Transfer	Grasp	Contact	Insert	Lift	Stack	Finish	Stack	Lift	Finish
DP (DDPM, CNN)	95.1 \pm 1.2	92.4 \pm 1.3	90.2 \pm 1.9	77.4 \pm 2.7	69.0 \pm 3.1	63.2 \pm 3.3	62.1 \pm 3.5	52.9 \pm 3.9	52.9 \pm 3.9	82.0 \pm 2.7	63.5 \pm 3.2	46.7 \pm 3.6
ACT	98.4 \pm 0.9	96.2 \pm 1.0	94.8 \pm 2.1	81.3 \pm 2.6	73.5 \pm 3.0	68.1 \pm 3.2	66.7 \pm 3.6	57.5 \pm 4.0	57.5 \pm 4.0	85.8 \pm 2.8	67.3 \pm 3.4	50.4 \pm 3.8
NL-ACT	94.3 \pm 1.6	91.5 \pm 1.9	90.4 \pm 2.1	83.2 \pm 2.5	74.1 \pm 3.1	70.0 \pm 3.4	62.4 \pm 3.6	55.3 \pm 4.0	55.3 \pm 4.0	82.3 \pm 3.0	65.2 \pm 3.3	48.4 \pm 3.4
HACT-Vq	98.5 \pm 0.9	97.6 \pm 1.2	96.2 \pm 1.4	87.4 \pm 2.4	82.2 \pm 2.7	76.3 \pm 2.8	79.2 \pm 2.2	68.5 \pm 3.1	68.5 \pm 3.1	90.6 \pm 2.3	76.1 \pm 2.8	55.8 \pm 3.2
InterACT	98.2 \pm 0.8	88.4 \pm 1.1	82.1 \pm 2.0	88.5 \pm 2.2	78.3 \pm 2.8	44.2 \pm 3.2	78.5 \pm 2.4	68.7 \pm 3.4	68.7 \pm 3.4	91.9 \pm 2.0	77.1 \pm 2.6	56.9 \pm 2.9
Ours	98.5 \pm 1.0	97.8 \pm 1.1	97.1 \pm 1.6	87.6 \pm 2.5	82.4 \pm 2.7	78.3 \pm 2.8	78.1 \pm 2.2	70.4 \pm 3.1	70.4 \pm 3.1	96.4 \pm 1.8	79.3 \pm 2.5	59.7 \pm 2.5

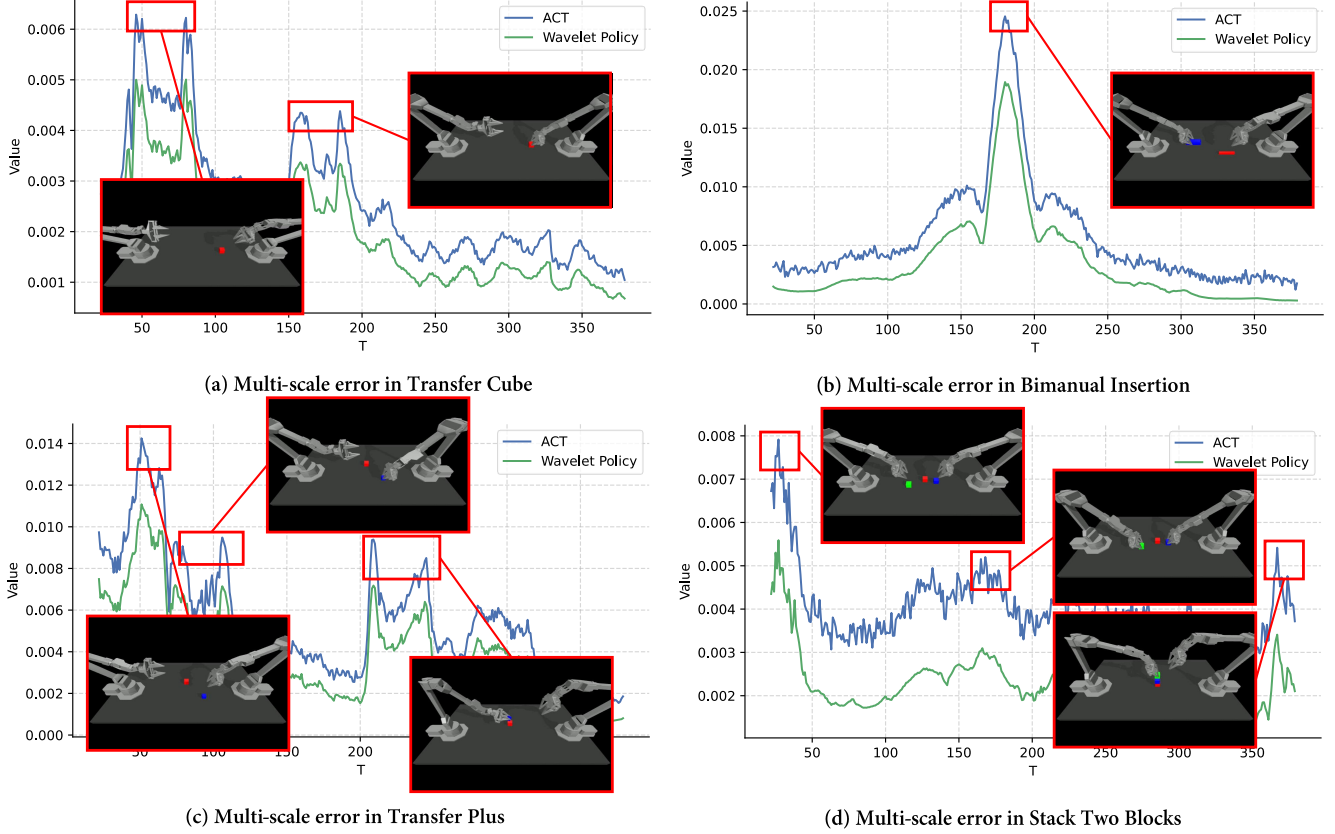


Fig. 4: Multi-scale error comparison between ACT and our Wavelet Policy on the four tasks.

 TABLE III: Per-frame inference average latency of Wavelet Policy and ACT under single- and dual-camera inputs. Latency (s/frame) \downarrow

Model	One Cam	Two Cam
Wavelet Policy	0.0308	0.0331
ACT	0.0390	0.0480

the SE2MD architecture allows transformers to effectively process these global features, enabling the model to fully leverage the benefits of frequency-domain representations.

Besides, we benchmark on-device latency. Without ONNX, PyTorch-only inference is slower, shown in Table VI. With ONNX Runtime shown in Table III, Wavelet Policy remains consistently faster than ACT for both one- and two-camera inputs. Together with the expected gains from TensorRT deployment [41], these results underscore superior potential for Wavelet Policy at edge deployment.

C. Feature Fusion in Embedding Dimension

In this experiment, we evaluated the impact of feature fusion on the embedding dimension compared to the ACT model. The ACT model is a classic embodiment of the traditional length-dimension fusion model in intelligent models. In Fig. 5, we present the experimental results by transforming them into progressively accumulated success rates. This visualization effectively illustrates how performance of each model evolves as task complexity increases and task volume expands. The results show that embedding dimension fusion is consistently superior to length-dimension fusion. As shown in TABLE. I, the multi-camera mode performance of this model achieves higher success rates with smaller model parameter growth, demonstrating higher efficiency and better task performance, especially in long-distance and high-difficulty tasks.

TABLE IV: Real-world evaluation: success rates [0.0, 1.0] on physical manipulation tasks.

	Stack Block			Store Strawberry			Store Lemon			Store Items			Assist Sewing			Stack Blocks		
	Grasp	Lift	Stack	Grasp	Lift	Place	Grasp	Lift	Place	First	Second	Finish	Contact	Feed	Align	Stack	Lift	Finish
ACT	0.8	0.7	0.6	0.9	0.8	0.7	0.7	0.6	0.6	0.8	0.6	0.5	0.8	0.8	0.6	0.6	0.5	0.4
Ours	0.9	0.8	0.8	1.0	0.9	0.8	0.9	0.8	0.7	0.9	0.8	0.7	0.8	0.8	0.7	0.8	0.7	0.7

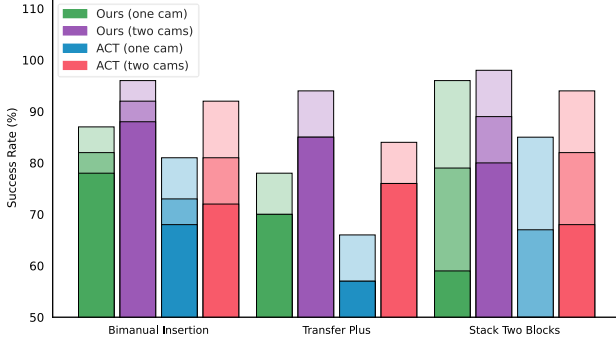


Fig. 5: Progressive accumulation of success rates across sub-tasks, illustrating how the performance of different models varies as task complexity increases.

D. Learnable Scale-Domain Filter

Next, we introduce Learnable Filters into our model. Fig. 6 presents the relationship between the success rate of the task and the value of N . As shown in TABLE V, it represents the individual parameter quantities of each filter with a latitude of 64 in the embedding layer. Adding learnable filters can controllably increase the model capacity. The results show that adding learnable filters improves performance, particularly in challenging tasks like Stack Two Blocks and Transfer Plus, where fine-grained motion adjustments are crucial.

Both RBF and RBLF demonstrated improvements in Transfer Plus and Stack Two Blocks, validating the effectiveness of residual learning. However, the overall performance gains were relatively modest. Unlike ResNet-based models, which undergo extended training on large-scale datasets to extract generalizable patterns, our model is trained on a single-task dataset, limiting its ability to capture task-agnostic features and thus constraining overall improvement. Among the evaluated filters, RBLF achieved the highest success rates across most tasks. This can likely be attributed to the stability of linear transformations in refining motion predictions. Particularly in long-horizon tasks such as Transfer Plus, linear layers offer a greater number of parameters compared to convolutional layers, enabling the model to learn higher-level motion representations more effectively. For EBF, we observe that it achieves superior performance in Stack Two Blocks, suggesting that element-wise scaling enhances fine-grained motion adjustments, which are critical in precision-demanding tasks.

TABLE V: Trainable parameters of single scale-domain filter with a latitude of 64 in the embedding layer.

	RBF	RBLF	EBF
# Params	0.0290 M	0.0042 M	0.0250 M

E. Real-World Evaluation

As shown in Fig. 3, the real-world task design aims to ensure a seamless bridge from simulation to hardware and facilitate edge deployment of the policy. Our task suite spans three robotic platforms: the Airbot Play academic arm from DISCOVER Robotics, and the xArm6 industrial manipulator from UFactory. In the industrial-arm setting, because a teleoperation robotic arm was unavailable at the factory, we collected training data using multiple conventional computer-vision pipelines across diverse visual conditions. As shown in TABLE IV, we report real-world task results averaged across two random seeds. Each seed is trained for 100k iterations on 100 demonstrations per task, with the best-performing checkpoint selected by validation performance. At test time, each seed is evaluated on five independent runs, and the final score is computed by averaging over the two seeds and their corresponding evaluation runs.

Comprehensive results demonstrate that Wavelet Policy consistently achieves higher success rates compared to baseline visuomotor policies, with improvements on tasks involving complex contact phases and multi-step object placement. Wavelet Policy was further validated on real-world robotic manipulation tasks to assess its robustness beyond simulation. The results indicate that incorporating wavelet-based multi-scale feature processing and the SE2MD architecture not only preserves efficiency in edge deployment but also enables reliable trajectory generation in real-world settings.

V. ABLATION STUDIES

In this ablation study, we design a comprehensive set of experiments to demonstrate the critical role of WT and SE2MD in Wavelet Policy. The results are shown in TABLE VI

A. WT: Wavelet Transform

We tested latency and task completion accuracy on the complete pipeline. HWT still offers the fastest inference at 0.0608 s per frame while achieving the best success rate across every sub-phase of both Bimanual Insertion and Transfer Plus. The short symmetric filter bior1.1 is only $\approx 2.8\%$ slower yet its average success rate drops by about 3 pp; longer 10-tap filters such as sym5, db5 and the high-regularity coif3 stretch the forward path by up to 45%.

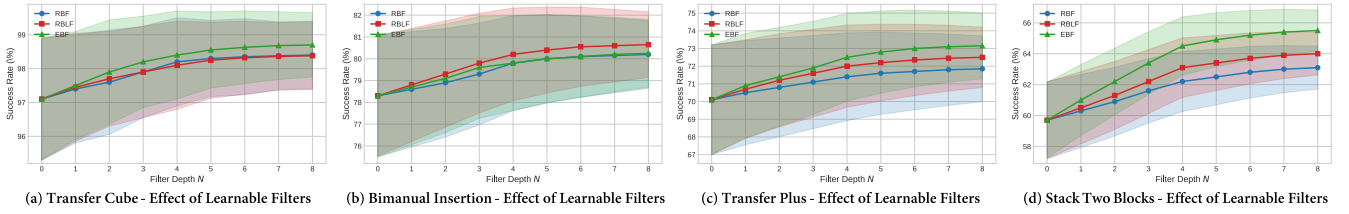


Fig. 6: The relationship between the success rate of the task and the value of N for the LSDF.

TABLE VI: Ablation study of WT and SE2MD architecture.

	Bimanual Insertion			Transfer Plus			Latency (s/frame)
	Grasp	Contact	Insert	Lift	Stack	Finish	
ACT	81.3 \pm 2.6	73.5 \pm 3.0	68.1 \pm 3.2	66.7 \pm 3.6	57.5 \pm 4.0	57.5 \pm 4.0	0.0784
haar	87.6 \pm 2.5	82.4 \pm 2.7	78.3 \pm 2.8	78.1 \pm 2.2	70.4 \pm 3.1	70.4 \pm 3.1	0.0608
db5	—	—	—	—	—	—	0.0796
bior1.1	86.0 \pm 2.6	80.1 \pm 3.0	75.0 \pm 3.1	75.9 \pm 2.6	67.0 \pm 3.3	67.0 \pm 3.3	0.0625
bior2.4	86.7 \pm 2.6	80.8 \pm 2.9	76.1 \pm 3.0	76.8 \pm 2.6	68.2 \pm 3.1	68.2 \pm 3.1	0.0732
rbio1.1	85.5 \pm 2.9	79.2 \pm 3.2	73.9 \pm 3.3	75.0 \pm 3.0	65.8 \pm 3.3	65.8 \pm 3.3	0.0716
coif3	—	—	—	—	—	—	0.0884
sym5	86.3 \pm 2.7	80.5 \pm 2.9	75.7 \pm 3.0	76.3 \pm 2.7	67.6 \pm 3.1	67.6 \pm 3.1	0.0813
w/o WT	49.4 \pm 2.6	31.8 \pm 2.7	14.4 \pm 3.5	41.2 \pm 2.1	9.5 \pm 3.1	9.5 \pm 3.1	0.0585
w/o SE2MD	44.8 \pm 2.5	31.2 \pm 2.8	11.4 \pm 3.2	37.5 \pm 2.3	8.5 \pm 3.4	8.5 \pm 3.4	0.0597

Although the biorthogonal families behave reasonably well during the Contact–Insert sub-phases, they still lag behind haar by 3–4 pp on the long-range Finish stage. The more complex db5 and coif3 filters cause gradient explosions and frequent loss oscillations in the SE2MD backbone; training never converges, so their final success rate is 0. Nevertheless, we can still time their forward pass, making it clear that these bases incur a high real-time cost without any payoff in task completion.

To single out importance of the wavelet transform, we entirely remove both DWT and IDWT. Doing so slightly reduces latency to 0.0585 s/frame, but devastates performance: the average success rate plummets from 83% to 32% on Bimanual Insertion and from 73% to 20% on Transfer Plus, a loss of more than 50 pp. These results highlight that WT supplies the crucial multi-scale time–frequency representation needed for fine-grained temporal control; removing it sacrifices precision at critical contact moments even though it shortens the computational graph.

B. SE2MD: Single Encoder to Multiple Decoders

To evaluate the effectiveness of SE2MD in our ablation study, we modify the framework by replacing the multiple-decoder structure with a single decoder. Specifically, instead of distributing wavelet-transformed features across multiple decoders, we concatenate all wavelet-transformed features and feed them into a single decoder. The decoder then disentangles the processed information before applying IDWT to reconstruct the output sequence. This setup allows us to assess the impact of the SE2MD architecture on temporal sequence modeling. The result shows that removing the SE2MD structure leads to a significant drop in success rates

across all tasks, with the most pronounced performance degradation observed in the Transfer task. This suggests that SE2MD plays a crucial role in extracting and distributing hierarchical temporal features, which are essential for the performance of Wavelet Policy.

VI. CONCLUSION AND LIMITATION

We have presented Wavelet Policy, a multi-scale robotic trajectory framework that integrates WT and the SE2MD architecture, achieving a parameter reduction of over threefold compared to smaller mainstream models. By decomposing visual data into distinct frequency bands, this approach captures both global and fine-grained details, ensuring robust performance in complex tasks. Our experiments on ten challenging robotic arm scenarios demonstrate significant accuracy gains over competing methods, including long-range tasks.

Wavelet Policy also has limitations. The current system is primarily vision-driven and can be sensitive to occlusions. As future work to address partial observability and improve contact robustness, we will integrate proprioceptive signals joint angles/velocities into SE2MD, fusing them with visual features via cross-modal attention. Besides, future work could involve a more precise integration of advanced methods for addressing Markov decision processes [42] and further explore filters design methods so that provide filter selection criteria

REFERENCES

- [1] C. Chi, Z. Xu, S. Feng, E. Cousineau, Y. Du, B. Burchfiel, R. Tedrake, and S. Song, “Diffusion policy: Visuomotor policy learning via action diffusion,” *The International Journal of Robotics Research*, p. 02783649241273668, 2023.

- [2] K. Rohling, "Integrating natural language instructions into the action chunking transformer for multi-task robotic manipulation." [Online]. Available: <https://github.com/krohling>
- [3] T. Z. Zhao, V. Kumar, S. Levine, and C. Finn, "Learning fine-grained bimanual manipulation with low-cost hardware," *arXiv preprint arXiv:2304.13705*, 2023.
- [4] Z. Zhao, Q. Wu, J. Wang, B. Zhang, C. Zhong, and A. A. Zhilenkov, "Exploring embodied intelligence in soft robotics: a review," *Biomimetics*, vol. 9, no. 4, p. 248, 2024.
- [5] T. Schmieg and C. Lanquillon, "Time series representation learning: A survey on deep learning techniques for time series forecasting," in *International Conference on Human-Computer Interaction*. Springer, 2024, pp. 422–435.
- [6] Z. Fu, T. Z. Zhao, and C. Finn, "Mobile aloha: Learning bimanual mobile manipulation with low-cost whole-body teleoperation," *arXiv preprint arXiv:2401.02117*, 2024.
- [7] A. C.-W. Lee, I. Chuang, L.-Y. Chen, and I. Soltani, "Interact: Inter-dependency aware action chunking with hierarchical attention transformers for bimanual manipulation," in *Conference on Robot Learning*. PMLR, 2025, pp. 1730–1743.
- [8] J. H. Park, W. Choi, S. Hong, H. Seo, J. Ahn, C. Ha, H. Han, and J. Kwon, "Hierarchical action chunking transformer: Learning temporal multimodality from demonstrations with fast imitation behavior," in *2024 IEEE/RSJ International Conference on Intelligent Robots and Systems (IROS)*. IEEE, 2024, pp. 12 648–12 654.
- [9] D. Zhang and D. Zhang, "Wavelet transform," *Fundamentals of image data mining: Analysis, Features, Classification and Retrieval*, pp. 35–44, 2019.
- [10] J. Hua, L. Zeng, G. Li, and Z. Ju, "Learning for a robot: Deep reinforcement learning, imitation learning, transfer learning," *Sensors*, vol. 21, no. 4, p. 1278, 2021.
- [11] S. Mahmoudi, A. Davar, P. Sohrabipour, R. B. Bist, Y. Tao, and D. Wang, "Leveraging imitation learning in agricultural robotics: a comprehensive survey and comparative analysis," *Frontiers in Robotics and AI*, vol. 11, p. 1441312, 2024.
- [12] N. Di Palo and E. Johns, "Keypoint action tokens enable in-context imitation learning in robotics," *arXiv preprint arXiv:2403.19578*, 2024.
- [13] K. Panaganti, Z. Xu, D. Kalathil, and M. Ghavamzadeh, "Distributionally robust behavioral cloning for robust imitation learning," in *2023 62nd IEEE Conference on Decision and Control (CDC)*. IEEE, 2023, pp. 1342–1347.
- [14] B. Lin, "Behavioral cloning and imitation learning," in *Reinforcement Learning Methods in Speech and Language Technology*. Springer, 2024, pp. 63–67.
- [15] Z. Li, R. Pérez-Dattari, R. Babuska, C. Della Santina, and J. Kober, "Beyond behavior cloning: Robustness through interactive imitation and contrastive learning," *arXiv preprint arXiv:2502.07645*, 2025.
- [16] K. Ruan, J. Zhang, X. Di, and E. Bareinboim, "Causal imitation learning via inverse reinforcement learning," in *The Eleventh International Conference on Learning Representations*, 2023.
- [17] M. Zare, P. M. Kebria, A. Khosravi, and S. Nahavandi, "A survey of imitation learning: Algorithms, recent developments, and challenges," *IEEE Transactions on Cybernetics*, 2024.
- [18] M. Seo, S. Han, K. Sim, S. H. Bang, C. Gonzalez, L. Sentis, and Y. Zhu, "Deep imitation learning for humanoid loco-manipulation through human teleoperation," in *2023 IEEE-RAS 22nd International Conference on Humanoid Robots (Humanoids)*. IEEE, 2023, pp. 1–8.
- [19] Y. Hu, F. J. Abu-Dakka, F. Chen, X. Luo, Z. Li, A. Knoll, and W. Ding, "Fusion dynamical systems with machine learning in imitation learning: A comprehensive overview," *Information Fusion*, p. 102379, 2024.
- [20] J. W. Kim, T. Z. Zhao, S. Schmidgall, A. Deguet, M. Kobilarov, C. Finn, and A. Krieger, "Surgical robot transformer (srt): Imitation learning for surgical tasks," *arXiv preprint arXiv:2407.12998*, 2024.
- [21] C. Ai, H. Yang, X. Liu, R. Dong, Y. Ding, and F. Guo, "Mtmol-gpt: De novo multi-target molecular generation with transformer-based generative adversarial imitation learning," *PLoS computational biology*, vol. 20, no. 6, p. e1012229, 2024.
- [22] A. Hu, G. Corrado, N. Griffiths, Z. Murez, C. Gurau, H. Yeo, A. Kendall, R. Cipolla, and J. Shotton, "Model-based imitation learning for urban driving," *Advances in Neural Information Processing Systems*, vol. 35, pp. 20 703–20 716, 2022.
- [23] Y. Cai, J. Gao, C. Pohl, and T. Asfour, "Visual imitation learning of task-oriented object grasping and rearrangement," in *2024 IEEE/RSJ International Conference on Intelligent Robots and Systems (IROS)*. IEEE, 2024, pp. 364–371.
- [24] A. Saadati, M. T. Masouleh, and A. Kalhor, "Deep learning-based imitation of human actions for autonomous pick-and-place tasks," in *2024 32nd International Conference on Electrical Engineering (ICEE)*. IEEE, 2024, pp. 1–7.
- [25] J. Hu, F. Wang, X. Li, Y. Qin, F. Guo, and M. Jiang, "Trajectory tracking control for robotic manipulator based on soft actor-critic and generative adversarial imitation learning," *Biomimetics*, vol. 9, no. 12, p. 779, 2024.
- [26] J. Lv, Q. Li, Q. Sun, and X. Wang, "T-conv: A convolutional neural network for multi-scale taxi trajectory prediction," in *2018 IEEE international conference on big data and smart computing (bigcomp)*. IEEE, 2018, pp. 82–89.
- [27] J. Lv, Q. Sun, Q. Li, and L. Moreira-Matias, "Multi-scale and multi-scope convolutional neural networks for destination prediction of trajectories," *IEEE Transactions on Intelligent Transportation Systems*, vol. 21, no. 8, pp. 3184–3195, 2019.
- [28] Z. Liu, C. Li, N. Yang, Y. Wang, J. Ma, G. Cheng, and X. Zhao, "Mstf: Multiscale transformer for incomplete trajectory prediction," in *2024 IEEE Intelligent Vehicles Symposium (IV)*. IEEE, 2024, pp. 573–580.
- [29] Z. Liu, C. Li, Y. Wang, N. Yang, X. Fan, J. Ma, and X. Zhao, "Multi-scale temporal fusion transformer for incomplete vehicle trajectory prediction," *IEEE Transactions on Intelligent Vehicles*, 2024.
- [30] Y. Ze, G. Zhang, K. Zhang, C. Hu, M. Wang, and H. Xu, "3d diffusion policy: Generalizable visuomotor policy learning via simple 3d representations," in *ICRA 2024 Workshop on 3D Visual Representations for Robot Manipulation*.
- [31] Z. Zhang, D. Guo, S. Zhou, J. Zhang, and Y. Lin, "Flight trajectory prediction enabled by time-frequency wavelet transform," *Nature Communications*, vol. 14, no. 1, p. 5258, 2023.
- [32] R. Azad, A. Kazerouni, A. Sulaiman, A. Bozorgpour, E. K. Aghdam, A. Jose, and D. Merhof, "Unlocking fine-grained details with wavelet-based high-frequency enhancement in transformers," in *International Workshop on Machine Learning in Medical Imaging*. Springer, 2023, pp. 207–216.
- [33] W. Zou, M. Jiang, Y. Zhang, L. Chen, Z. Lu, and Y. Wu, "Sdwnet: A straight dilated network with wavelet transformation for image deblurring," in *Proceedings of the IEEE/CVF international conference on computer vision*, 2021, pp. 1895–1904.
- [34] M. L. A. Sarna, M. R. Hossain, and M. A. Islam, "Comparative analysis of stft and wavelet transform in time-frequency analysis of non-stationary signals," *International Journal of Novel Research in Engineering and Science*, 2024.
- [35] M. C. Yesilli, J. Chen, F. A. Khasawneh, and Y. Guo, "Automated surface texture analysis via discrete cosine transform and discrete wavelet transform," *Precision Engineering*, vol. 77, pp. 141–152, 2022.
- [36] S. Wagner, C. Ewald, D. Freitag, K.-H. Herrmann, A. Koch, J. Bauer, T. J. Vogl, A. Kemmling, and H. Gufler, "Effects of tetrahydrolipstatin on glioblastoma in mice: Mri-based morphologic and texture analysis correlated with histopathology and immunochemistry findings—a pilot study," *Cancers*, vol. 16, no. 8, p. 1591, 2024.
- [37] G. S. Kumar and M. L. P. Rani, "Image compression using discrete wavelet transform and convolution neural networks," *Journal of Electrical Engineering & Technology*, vol. 19, no. 6, pp. 3713–3721, 2024.
- [38] A. K. Umam, P. T. B. Ngastiti, A. Alfian, Z. Shahadah, and A. F. Muamalah, "The application of discrete wavelet transform for digital image compression," *Jurnal Matematika Sains dan Teknologi*, vol. 25, no. 1, pp. 01–08, 2024.
- [39] D. Grochala, R. Grzejda, A. Parus, and S. Berczyński, "The wavelet transform for feature extraction and surface roughness evaluation after micromachining," *Coatings*, vol. 14, no. 2, p. 210, 2024.
- [40] B. Cansiz, C. U. Kilinc, and G. Serbes, "Tunable q-factor wavelet transform based lung signal decomposition and statistical feature extraction for effective lung disease classification," *Computers in Biology and Medicine*, vol. 178, p. 108698, 2024.
- [41] A. Kasoju and T. Vishwakarma, "Optimizing transformer models for low-latency inference: Techniques, architectures, and code implementations," *International Journal of Science and Research (IJSR)*, vol. 14, pp. 857–866, 2025.
- [42] G. Di Gennaro, A. Buonanno, F. Verolla, G. Fioretti, F. A. Palmieri, and K. R. Pattipati, "Imitation learning through prior injection in markov decision processes," in *Applications of Artificial Intelligence and Neural Systems to Data Science*. Springer, 2023, pp. 103–113.